Journal of Zhejiang University-SCIENCE B 2026 27(7):761-774
www.jzus.zju.edu.cn; www.springer.com/journal/11585
E-mail: jzus_b@zju.edu.cn

Research Article
https://doi.org/10.1631/jzus.B2500787

Check for updates

Dual-functional nanoplatform for simultaneous degradation of circRNA *CDR1as* and real-time monitoring of miR-7 in live cells

Yan HUANG[1], Jialin YE[1], Lan XU[1], Xingjie HU[2]✉, Nan CHEN[1]✉

[1]*College of Chemistry and Materials Science, The Education Ministry Key Lab of Resource Chemistry, Shanghai Engineering Research Center of Green Energy Chemical Engineering, and Shanghai Frontiers Science Center of Biomimetic Catalysis, Shanghai Normal University, Shanghai 200234, China*
[2]*School of Public Health, Shanghai Jiao Tong University School of Medicine, Shanghai 201318, China*

Abstract: Circular RNAs (circRNAs) are key post-transcriptional regulators with critical roles in pathogenesis, yet existing tools for their precise manipulation and functional analysis in living cells remain to be developed. A compelling therapeutic target in this field is the circRNA cerebellar degeneration-related protein 1 antisense (*CDR1as*), functioning as an oncogenic sponge for microRNA-7 (miR-7). Herein, we report a novel multifunctional zeolitic imidazolate framework-8 (ZIF-8)-based nanoplatform for the simultaneous disruption and real-time monitoring of the *CDR1as*/miR-7 regulatory axis. This system, named DZ/MB@ZIF-8, co-encapsulates a designed set of DNAzymes (DZs) for the catalytic cleavage of *CDR1as* as well as a molecular beacon (MB) for reporting on miR-7 activity. Following cellular uptake and lysosomal trafficking, the acidic microenvironment triggers nanoplatform disassembly, concurrently releasing the therapeutic and sensing components along with essential Zn^{2+} cofactors for DZ activation. This system demonstrates efficient *CDR1as* degradation, which liberates miR-7 and inhibits the expression of its downstream oncogenic targets. Crucially, this therapeutic effect is directly correlated with a turn-on fluorescent signal from the MB, enabling the real-time, live-cell readout of circRNA regulation. This work establishes a versatile theranostic strategy that merges targeted gene regulation with intrinsic biosensing, offering a powerful platform for probing circRNA function and advancing RNA-based therapeutics.

Key words: Circular RNA (circRNA); Zeolitic imidazolate framework-8 (ZIF-8); MicroRNA-7 (miR-7); DNAzyme; Gene regulation

1 Introduction

Circular RNAs (circRNAs) are a type of non-coding RNA with a covalently closed circular structure (Wu et al., 2024). They are structurally distinct from linear messenger RNAs (mRNAs) and show higher stability in cells (Jeck et al., 2013). In the past decade, circRNAs have become a research hotspot due to their important role in gene regulation (Jeck et al., 2013; Yang et al., 2018; Liu and Chen, 2022; Chen et al., 2025). Among them, cerebellar degeneration-related protein 1 antisense (*CDR1as*), also known as *ciRS-7*, is one of the earliest discovered and most extensively studied circRNAs (Meng et al., 2020). It contains more than 70 microRNA-7 (miR-7)-binding sites and can act as a "molecular sponge" to adsorb miR-7, thereby regulating the expression of downstream target genes (Piwecka et al., 2017; Breuer et al., 2022; Shao et al., 2023). Studies have shown that *CDR1as* is abnormally expressed in various cancers (e.g., gastric cancer, breast cancer, and glioma cells) and participates in the occurrence, development, and metastasis of tumors through the miR-7-related pathways (Chen et al., 2019; Xu et al., 2025). Furthermore, the expression level of *CDR1as* is significantly correlated with the clinical stage and prognosis of cancer patients, demonstrating its potential as both a diagnostic marker and a therapeutic target for cancer (Shao et al., 2023; Xu et al., 2025).

By interfering with the expression of circRNAs, we can better understand their functions and assist in

✉ Nan CHEN, nchen@shnu.edu.cn
Xingjie HU, huxingjie@shsmu.edu.cn
Nan CHEN, https://orcid.org/0000-0001-8536-6631
Xingjie HU, https://orcid.org/0000-0002-0271-3843

Received Dec. 1, 2025; Revision accepted Apr. 8, 2026; Crosschecked June 23, 2026

© Zhejiang University Press 2026

curbing the progression of diseases related to circRNAs, including cancers. Various circRNA manipulation technologies have emerged as tools for intervention in circRNAs (Yang et al., 2021; Liu et al., 2022; Wang et al., 2023; Zhang et al., 2023). For example, small interfering RNA (siRNA) or short hairpin RNA (shRNA) targeting the degradation of *CDR1as*, is applicable to pathological conditions (such as neuroinflammation) caused by its overexpression (Ruda et al., 2014; Zhang et al., 2022; Singh et al., 2024). Artificial circRNA or microRNA (miRNA) antagonists are designed to precisely regulate downstream pathways (Liu et al., 2021; Mao et al., 2021). More recently, clustered regularly interspaced short palindromic repeats (CRISPR)/CRISPR-associated protein (Cas) systems have been introduced to precisely edit *CDR1as* expression (Bloomer et al., 2022; Song et al., 2023). However, technical limitations hinder the further development and clinical application of these strategies, such as the cost and instability of synthetic RNA molecules, the low efficiency of intracellular delivery, and the complex protein components required in CRISPR-Cas systems (Behr et al., 2021). Thus, new, simple, efficient, and low-cost regulatory strategies for circRNAs need to be developed. As a catalytically active DNA molecule, DNAzyme (DZ) has become an important tool for RNA research and application due to its high specificity and efficiency (Li et al., 2025; Liu et al., 2025): the high catalytic activity of DZ makes it an ideal signal amplifier for RNA detection. Scholars have developed various DZ-based circRNA detection methods, yet the direct utilization of DZ for cleaving circRNA has rarely been reported (McConnell et al., 2021; Yu and Zhao, 2023; Feng et al., 2025). DZ activation requires divalent metal ions such as magnesium, manganese, and zinc. However, the endogenous metal ion concentrations are insufficient, which restricts its application in living cells (Victor et al., 2018; Fan et al., 2021). In addition, the intracellular delivery and release efficiency of DZ need to be further improved for circRNA cleavage (Wang et al., 2019; Wu et al., 2022; Lee et al., 2023).

To evaluate the downregulation and therapeutic efficiency, it is necessary to extract RNA and analyze the expression levels of *CDR1as*, miR-7, and downstream genes by reverse transcription quantitative polymerase chain reaction (RT-qPCR) (Li et al., 2023; Odame et al., 2023). This process is cumbersome and time-consuming, but more importantly, it is unable to assess the therapeutic effect in real time and adjust accordingly. MiR-7 is the major effector of *CDR1as* in exerting its regulatory function, and the degradation of *CDR1as* will increase the intracellular abundance of miR-7 (Mehta et al., 2023; Wightman et al., 2024). Therefore, if the intracellular miR-7 level can be characterized in real time and visually, it can indirectly reflect the cleavage efficiency and therapeutic effect of *CDR1as*.

Zeolitic imidazolate framework-8 (ZIF-8) has emerged as a promising nanocarrier for DZs due to its unique properties (Troyano et al., 2019; Zhao et al., 2023; Zeng et al., 2024). Studies have shown that ZIF-8 can encapsulate various biomolecules and maintain their activity, ensuring biocompatibility under physiological conditions (Zhang et al., 2021; Wei et al., 2023; Gao et al., 2025). ZIF-8 is known to degrade under acidic conditions, which are typically found in intracellular compartments such as endosomes and lysosomes (Mishra et al., 2023). This degradation releases the encapsulated DZs in a controlled manner, ensuring that they reach their target site in an active form. Moreover, ZIF-8 serves as an intrinsic Zn^{2+} source, which is essential for the catalytic activity of DZs (Ye et al., 2021; Wu et al., 2022). This dual role of ZIF-8 as both a carrier and a cofactor source is particularly advantageous in Zn^{2+}-dependent DZ-based therapeutic applications.

In this study, we designed a ZIF-8-based nanoplatform co-encapsulating *CDR1as*-targeting DZs and a miR-7-targeting molecular beacon (MB) (DZ/MB@ZIF-8). After endocytosis, DZ/MB@ZIF-8 is encapsulated into lysosomes and disintegrated. With the help of Zn^{2+}, activated DZs can effectively cleave *CDR1as*. Real-time visualization of intracellular miR-7 is achieved via the fluorescence of an MB probe. Furthermore, the regulatory effects of the *CDR1as*/miR-7/mRNA axis are confirmed by subsequent inhibition of downstream genes regulated by miR-7, including *Raf-1* proto-oncogene, serine/threonine kinase (*RAF1*) and phosphatidylinositol-4,5-bisphosphate 3-kinase catalytic subunit delta (*PIK3CD*). This dual functional DZ/MB@ZIF-8 nanoplatform achieves simultaneous circRNA regulation and real-time monitoring in living cells, providing a novel approach to exploring the biological process and therapeutic regulation of circRNAs (Fig. 1).

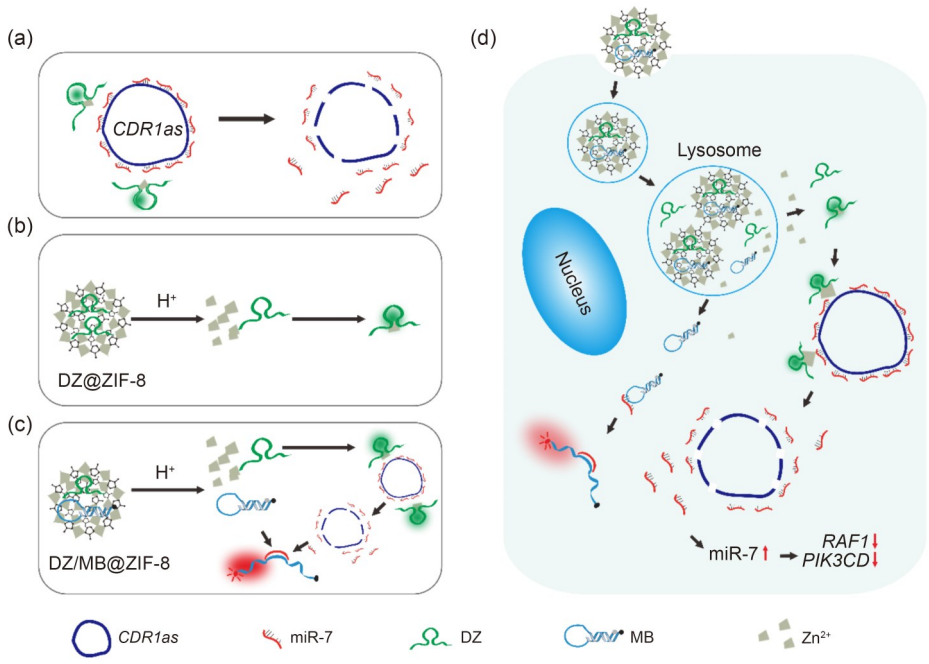


Fig. 1 Schematic illustration of the dual-functional DZ/MB@ZIF-8 nanoplatform for regulating and sensing the *CDR1as*/miR-7 axis. (a) DZs are designed to recognize and cleave *CDR1as*. (b) The acidic environment triggers the disassembly of DZ@ZIF-8, resulting in the release of DZ and Zn^{2+} ions to form activated DZ. (c) The degradation of DZ/MB@ZIF-8 releases DZ, MB, and Zn^{2+} cofactors, leading to DZ activation and *CDR1as* cleavage. The binding of the freed miR-7 to the MB generates a fluorescent signal. (d) Following cellular uptake and lysosomal trafficking, DZ/MB@ZIF-8 is disassembled. The released Zn^{2+} activates DZ, which then cleaves *CDR1as*. This frees miR-7, which can in turn inhibit the expression of its downstream target genes (e.g., *RAF1* and *PIK3CD*). The simultaneous binding of the freed miR-7 to the MB generates a fluorescent signal, providing a real-time readout of the platform's therapeutic activity. DZ: DNAzyme; MB: molecular beacon; ZIF-8: zeolitic imidazolate framework-8; *CDR1as*: cerebellar degeneration-related protein 1 antisense; miR-7: microRNA-7; *RAF1*: *Raf-1* proto-oncogene, serine/threonine kinase; *PIK3CD*: phosphatidylinositol-4,5-bisphosphate 3-kinase catalytic subunit delta.

2 Results and discussion

2.1 Design and in vitro validation of *CDR1as*-targeting DNAzyme set

CDR1as has a unique reverse splicing structure that distinguishes it from its cognate linear *CDR1* mRNA. DZs are capable of specifically recognizing the back-splice junction (BSJ) sequence of *CDR1as*, avoiding interference from homologous linear RNAs. We chose 8-17 DZ and 10-23 DZ, two DZs that have been widely used in mRNA regulation, and tested their ability to cleave *CDR1as*. The 8-17 DZ is a type of Zn^{2+}-dependent DZ that cleaves the rA–rG base junctions of RNA substrates (Santoro and Joyce, 1997; Cepeda-Plaza and Peracchi, 2020), while the 10-23 DZ is a type of Mg^{2+}-dependent DZ that cleaves the rR–rY (where R is A or G, and Y is U or C) base junctions of RNA substrates (Santoro and Joyce, 1997; Schubert, 2003). DZs consist of a two-sided binding arm for substrate RNA recognition and a middle sequence that forms the cleavage center upon the binding and activation of metal ions. The BSJ sequence is essential for circular *CDR1as* formation, and hence DNAzyme 1 (DZ1) targeting that region was designed. To ensure and enhance the cleavage efficiency of *CDR1as*, additional DZ-targeting sequences outside of BSJ were introduced. We designed both a DZ2-targeting sequence close to BJS and a DZ3-targeting sequence far from BJS (Figs. 2a, 2b, S1a, and S1b, and Table S1).

Based on the cleavage principle of DZ, its secondary structure must align with the corresponding catalytic domain (Nurmi et al., 2024). We used the RNAstructure software (version 6.4, Mathews Lab) to predict the secondary structure formed by the binding of the three DZs to the substrate RNA (Zuker, 2003;

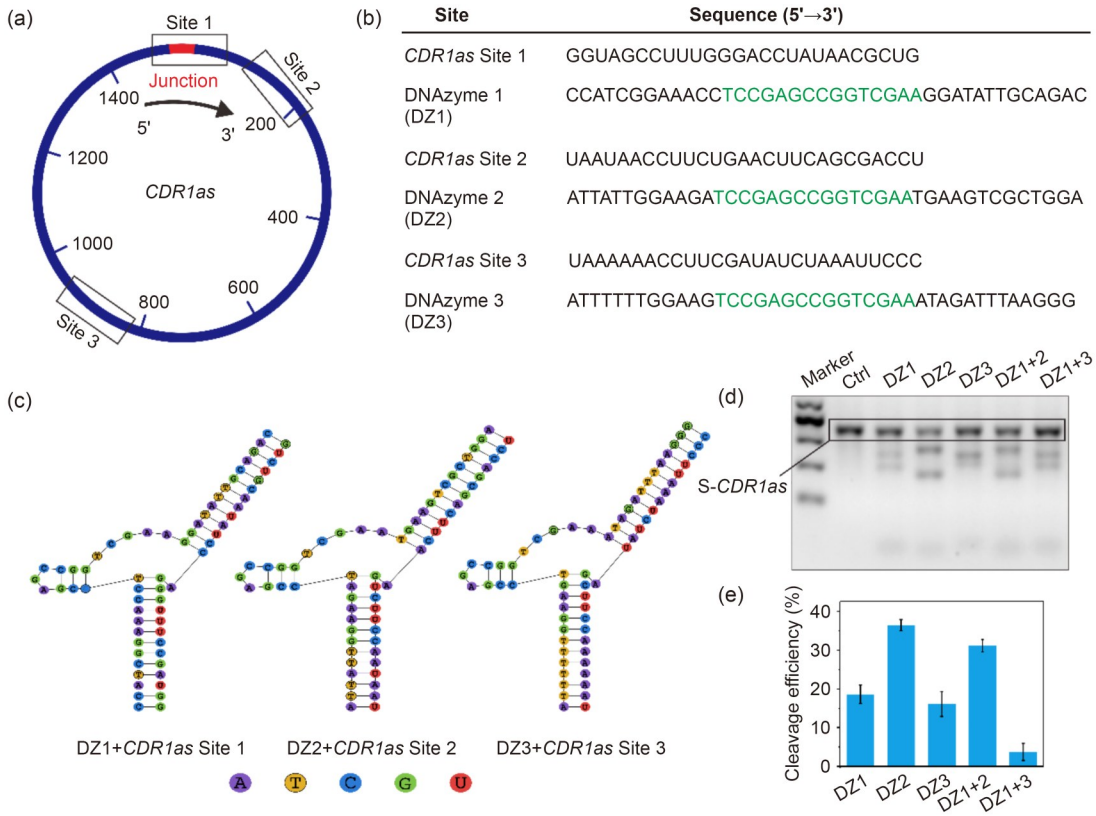


Fig. 2 Design and cleavage activity of DZs targeting *CDR1as*. (a) Schematic representation of *CDR1as* and the three cleavage sites (Site 1, Site 2, and Site 3) recognized by 8-17 DZ. (b) Sequences of the three cleavage sites. The catalytic core of the DZ is shown in green. (c) Predicted secondary structures of the DZ-target complexes using RNAstructure software. (d) Gel electrophoresis analysis of the cleavage of DZ and S-*CDR1as*. (e) Cleavage efficiency of individual or combined DZs was quantified using ImageJ software. The data are expressed as mean±SD (*n*=3). DZ: DNAzyme; Crtl: control; *CDR1as*: cerebellar degeneration-related protein 1 antisense; S-*CDR1as*: substrate RNA derived from *CDR1as* containing three DZ-targeted sequences; SD: standard deviation.

Agarwal et al., 2015; Sato et al., 2021). All three 8-17 DZs successfully attached to the targeted sequence substrates and formed specific secondary structures of catalytic domains (Fig. 2c). To investigate the interaction and cleavage effects of the designed DZs, three RNA sequences derived from *CDR1as* and the three DZ sites therein were concatenated to form a 783-nucleotide-long RNA, S-*CDR1as*, serving as an in vitro RNA mimic of *CDR1as* (Fig. S1c and Table S2). Three 8-17 DZs, either individually or as a combination, were separately incubated with the substrate in the presence of Zn^{2+}, and their nucleic acid cleavage efficiency was examined and compared using gel electrophoresis. Upon treatment with DZs, the intensity of the bands of *CDR1as* was reduced and short RNA fragments were observed, indicating RNA recognition and cleavage by the designed 8-17 DZs (Figs. 2d and 2e). Quantitative analysis pointed to DZ2 as the most powerful single DZ for *CDR1as* cleavage. This superior efficiency can be attributed to its favorable structural context. The target site of DZ2 is located near the 5' region of the circRNA, which possesses relatively low secondary structure complexity. In contrast, DZ1 targets the highly constrained BSJ, and DZ3 is situated in a region densely populated with miR-7-binding sites that likely create steric hindrance due to interactions with RNA-binding proteins (Hansen et al., 2013; Ashwal-Fluss et al., 2014; Shafaghat et al., 2025). Furthermore, the combined DZ set of DZ1+2 is more efficient than BSJ-targeting DZ1 alone, demonstrating a synergistic effect (Figs. 2d and 2e). This is likely due to the spatial proximity of Site 1 and Site 2 within the three-dimensional (3D) structure of *CDR1as*, allowing for a "cooperative cleavage" effect where initial cleavage by DZ1 alters local RNA folding, rendering Site 2 more accessible for DZ2.

Similarly, three 10-23 DZs targeting the *CDR1as* sequence—at BSJ (DZ1), close to (DZ2) or far from (DZ3)

BJS—were designed and synthesized (Figs. S2a–S2c). Individual DZs or DZ combinations were incubated with the *CDR1as* mimic RNA in the presence of Mg^{2+}, and their nucleic acid cleavage efficiency was determined by gel electrophoresis. The gel and quantitative analysis results were highly consistent with those obtained with 8-17 DZ. Combined DZ sets of DZ1+2 showed more efficient cleavage than other DZ combinations (Figs. S2d and S2e). These results demonstrated that both 8-17 DZ and 10-23 DZ could cleave *CDR1as* in vitro, and DZs targeting different parts of *CDR1as* exhibited differences in activity. Thus, combining the BSJ-targeting DZ1 with a DZ that recognizes the sequence in proximity may significantly enhance the ability to degrade and inhibit *CDR1as*.

2.2 DNAzyme-mediated regulation of the *CDR1as*/miR-7/*RAF1* and *PIK3CD* axes

Having confirmed the effectiveness of the designed DZ in cleaving *CDR1as* in vitro, the functionality of DZ in live cells was assessed. We hypothesized that DZ could cleave *CDR1as* and disrupt the miR-7 adsorption sponge. The results showed that increased intracellular miR-7 inhibited the expression of downstream genes (Fig. 3a). Individual DZs or their combinations were transfected into MCF-7 cells via a transfection reagent. After 48 h of co-incubation in the presence of 0.5 mmol/L Zn^{2+}, the RNA levels of *CDR1as* were assessed by RT-qPCR. All DZ-treated cells showed a significant decrease in *CDR1as* levels, and the combination of DZ1+2 appeared to be the most effective inhibitor of *CDR1as* (Fig. 3b). This result validated that DZ could serve as a potent tool for cleaving and regulating intracellular circRNAs. Next, we investigated whether the cleavage of *CDR1as* can regulate its downstream gene pathways. Research in osteosarcoma cells has shown that *CDR1as* regulates the expression of cancer-related genes, such as *PIK3CD* and *RAF1* through miR-7 (Xu et al., 2018). We also identified the miR-7-pairing sequence in the coding regions of *RAF1* and *PIK3CD* mRNAs using TargetScan software (Shafaghat et al., 2025), suggesting that these genes are directly regulated by miR-7 (Fig. S3). To investigate their responsiveness to miR-7 in MCF-7 cells,

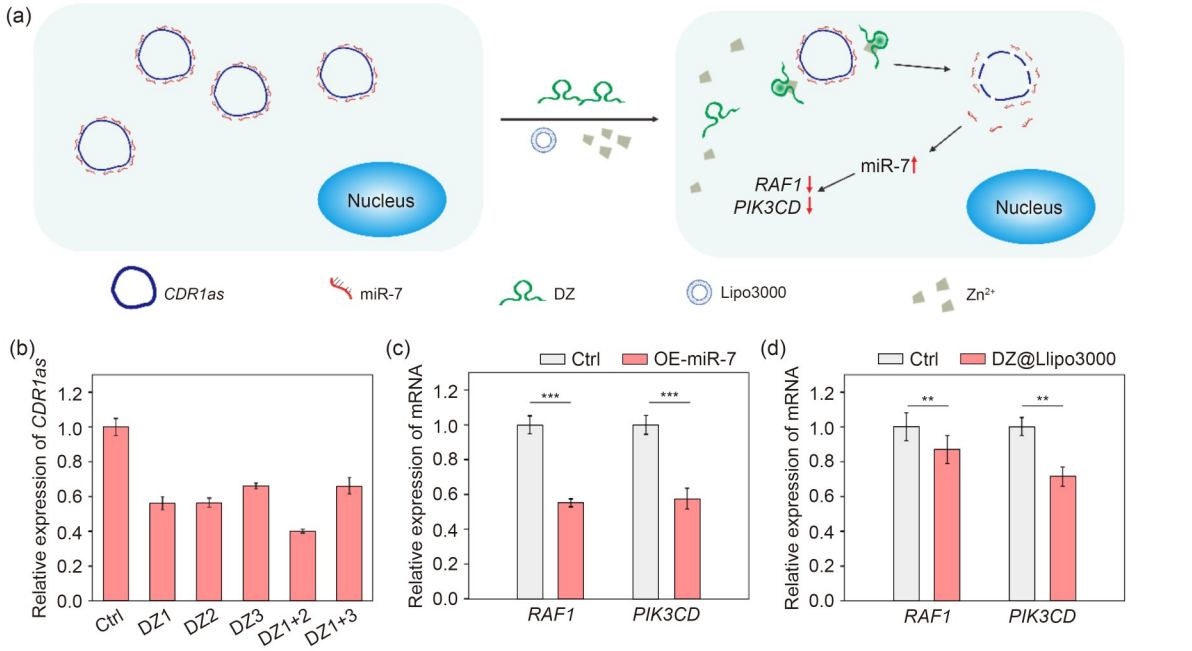


Fig. 3 DZ-mediated regulation of the *CDR1as*/miR-7/*RAF1* and *PIK3CD* axes. (a) Schematic diagram showing the DZ-mediated regulation of *CDR1as* and the downstream gene network. (b) Expression levels of *CDR1as* upon the indicated DZ treatment as quantified by RT-qPCR. (c) mRNA levels of *RAF1* and *PIK3CD* upon miR-7 overexpression as quantified by RT-qPCR. (d) mRNA levels of *RAF1* and *PIK3CD* under DZ (DZ1+2) treatment as quantified by RT-qPCR. Data are expressed as mean±SD (n=3). ** P<0.01 and *** P<0.001, compared with the control group. DZ: DNAzyme; miR-7: microRNA-7; *CDR1as*: cerebellar degeneration-related protein 1 antisense; Lipo3000: Lipofectamine 3000; OE-miR-7: overexpressed miR-7; *RAF1*: *Raf-1* proto-oncogene, serine/threonine kinase; *PIK3CD*: phosphatidylinositol-4,5-bisphosphate 3-kinase catalytic subunit delta; Ctrl: control; RT-qPCR: reverse transcription quantitative polymerase chain reaction.

exogenously synthesized miR-7 was overexpressed (OE-miR-7) in MCF-7 cells, and the expression levels of *RAF1* and *PIK3CD* were determined. A significant downregulation of both *RAF1* and *PIK3CD* was observed, confirming them as downstream genes regulated by the *CDR1as*/miR-7 axis (Fig. 3c). We then transfected the cells with the optimal combination of DZ1+2 (indicated as DZ) and observed decreased mRNA levels of *RAF1* and *PIK3CD* (Fig. 3d). The above results proved that the DZ delivered via a standard transfection reagent could effectively knock down *CDR1as* in MCF-7 cells and thereby cause a decrease in *RAF1* and *PIK3CD* mRNA levels, validating the proposed pathway.

2.3 Synthesis and characterization of the DZ@ZIF-8 nanocomplex

Next, we designed and constructed a nanocomplex to deliver DZ into mammalian cells. ZIF-8 is a type of zinc-based metal-organic framework (MOF) material with mild synthesis conditions, suitable for the carrier and intracellular delivery of biomolecules such as proteins and nucleic acids. ZIF-8 can disintegrate in the acidic environment of lysosomes and release bioactive cargos. In particular, the released zinc ions can serve as essential cofactors to activate 8-17 DZs. Therefore, ZIF-8 was chosen as the nanocarrier for DZ intracellular delivery in the next step (Fig. 4a). ZIF-8 nanoparticles were synthesized by rapid colloidal chemistry at room temperature, and then DZs were loaded onto the surface of ZIF-8 by electrostatic adsorption, forming DZ@ZIF-8 nano-complexes. Scanning electron microscopy (SEM) analysis revealed that the synthesized ZIF-8 nanoparticles exhibited a hexagonal shape, with an average size of (92.8±3.5) nm (Figs. S4a and S4b). After the adsorption of DZ on the ZIF-8 surface, the original polygonal angles became smoother, and the particle size increased to (96.6±4.6) nm (Figs. 4b and 4c). The hydration radius was determined using dynamic light scattering (DLS): it increased from 122.4 nm for ZIF-8 to 164.2 nm for DZ@ZIF-8 (Fig. S4c). Zeta potential analysis showed that the surface charge changed from +15 mV for ZIF-8 to −21 mV for DZ@ZIF-8 (Fig. 4d). The loading of DZ on ZIF-8 was examined by differential subtraction fluorescence, and the loading efficiency was up to 55.54 μg/mg (Figs. S4d and S4e). The biocompatibility of DZ@ZIF-8 was determined by methylthiazolyldiphenyl-tetrazolium bromide (MTT) assays, and its toxicity at ⩽30 μg/mL was negligible (Fig. S4f). To ensure its suitability for biological applications, the colloidal and structural stability of the nanoplatform was evaluated. DZ@ZIF-8 nanoparticles were incubated in an aqueous solution for 7 d. The hydrodynamic size and polydispersity index (PDI) remained relatively constant (Fig. S5a), indicating excellent colloidal stability. Furthermore, no significant fluorescence from cyanine 3 (Cy3)-labeled cargo was detected in the supernatant over a 24-h period (Fig. S5b), confirming that the DNA probes had been stably encapsulated within the ZIF-8 framework without premature leakage in physiological media. To investigate the intracellular delivery of DZ by ZIF-8, DZ labeled with Alexa Fluor 647 (Alexa647) was utilized to construct fluorescent DZ@ZIF-8. Both Alexa647-DZ@ZIF-8 and free Alexa647-DZ were incubated with MCF-7 cells for 24 h, and the intracellular fluorescence was observed using a Leica TCS SP8 confocal microscope (Leica Microsystems, Wetzlar, Germany). Obvious fluorescence was detected in cells treated with Alexa647-DZ@ZIF-8, while no fluorescence was detected in cells incubated with free Alexa647-DZ (Fig. 4e). This result validated ZIF-8 as an effective nanocarrier for the intracellular delivery of nucleic acids.

The key step for DZ@ZIF-8 to exert its expected function within cells is disintegration within acidic lysosomes (Fig. 5a). The responsiveness of DZ@ZIF-8 to acidic conditions was investigated by incubating it in solutions at either pH 7.4 or 5.5 for 2 h. The mixture was then centrifuged, and the supernatant was analyzed by gel electrophoresis. A DZ band appeared in the sample supernatant at pH 5.5, while no such band was detected at pH 7.4, indicating that the degradation of DZ@ZIF-8 occurred only at pH 5.5 (Fig. S5c). Importantly, the fluorescence properties of Cy3-DZ remained stable across different pH buffers (Fig. S5d), confirming that the degradation of the material in an acidic lysosomal environment does not affect the fluorescence of Cy3 and ensuring the accuracy of subsequent intracellular detection of miR-7. Furthermore, supernatants at different pH values were applied to S-*CDR1as* to compare their enzymatic activity in vitro. Similarly, only the sample supernatant at pH 5.5 could cleave S-*CDR1as* (Fig. 5b), validating the functionality of DZs and Zn^{2+} released from DZ@ZIF-8.

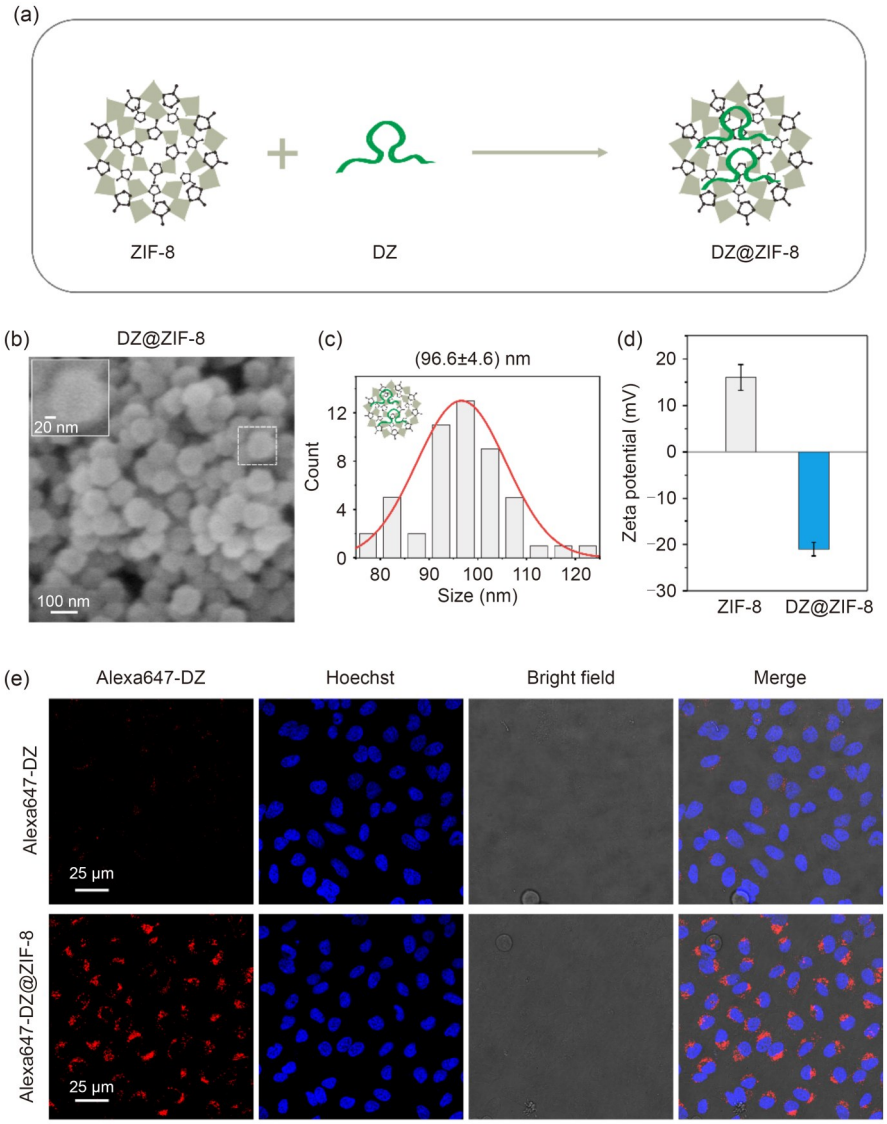


Fig. 4 Synthesis and characterization of the DZ@ZIF-8 nanocomplex. (a) Schematic of the DZ-loaded ZIF-8 nanoparticle (DZ@ZIF-8). (b, c) SEM images and corresponding particle size distribution analysis of DZ@ZIF-8. The inset in (b) is a magnified view of the area indicated by the white dashed box. (d) Zeta potentials of ZIF-8 and DZ@ZIF-8. The data are expressed as mean±SD (*n*=3). (e) Cells were incubated with Alexa647-DZ or Alexa647-DZ@ZIF-8 for 24 h and imaged by confocal microscopy (Alexa647: red; Hoechst: blue). DZ: DNAzyme; ZIF-8: zeolitic imidazolate framework-8; SEM: scanning electron microscopy; SD: standard deviation.

Subsequently, the intracellular disintegration of DZ@ZIF-8 was investigated. Alexa647-DZ@ZIF-8 was incubated with MCF-7 cells for 16 h before observation using a confocal microscope, and obvious intracellular fluorescence was detected. Importantly, the fluorescence of Alexa647-DZ showed significant colocalization with stained lysosomes, implying that DZ@ZIF-8 accumulated in lysosomes following endocytosis. Cells were then incubated with fresh medium for another 2 h and examined by confocal imaging. The colocalization ratio between Alexa647 and Lysotracker dropped from 69% to 31%, indicating the rapid lysosomal escape of DZ following DZ@ZIF-8 degradation (Figs. 5c and 5d).

We next investigated the intracellular cleavage of *CDR1as* by DZ@ZIF-8. Individual DZ1, DZ2, DZ3, or their combinations were used to construct DZ@ZIF-8 nanoparticles. These nanoparticles were then incubated with MCF-7 cells for 48 h before quantifying *CDR1as* by RT-qPCR. The RNA levels of *CDR1as* decreased

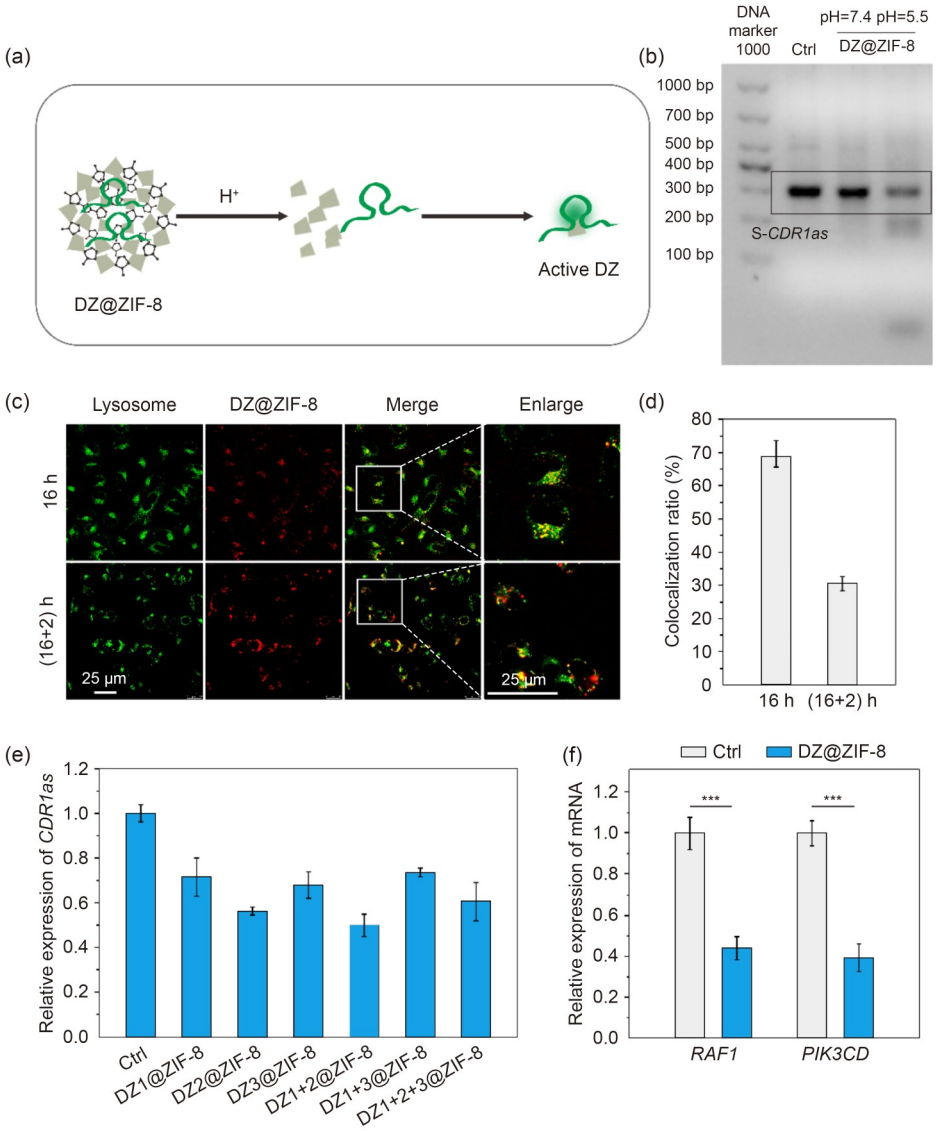


Fig. 5 Regulation of *CDR1as* and downstream genes by DZ@ZIF-8. (a) Schematic of acidic degradation of DZ@ZIF-8 and DZ activation. (b) Gel electrophoresis analysis of *CDR1as* cleavage under various pH conditions. (c) Lysosomal colocalization of Alexa647-DZ@ZIF-8 (30 μg/mL) was observed by confocal microscopy following a 16-h incubation and LysoTracker green staining (lysosome: green; DZ@ZIF-8: red). (d) Colocalization ratio of Alexa647-DZ@ZIF-8 with lysosomes quantified using ImageJ software (*n*=20 cells). (e) RNA levels of *CDR1as* upon treatment with DZ-loaded ZIF-8 determined by RT-qPCR (*n*=3). (f) RT-qPCR analysis of the mRNA levels of *RAF1* and *PIK3CD* treated with DZ@ZIF-8 (*n*=3). Data are expressed as mean±SD. * *P*<0.001. *CDR1as*: cerebellar degeneration-related protein 1 antisense; ZIF-8: zeolitic imidazolate framework-8; DZ: DNAzyme; mRNA: messenger RNA; RT-qPCR: reverse transcription quantitative polymerase chain reaction; Ctrl: control; *RAF1*: *Raf-1* proto-oncogene, serine/threonine kinase; *PIK3CD*: phosphatidylinositol-4,5-bisphosphate 3-kinase catalytic subunit delta.**

in all DZ@ZIF-8-treated cells. Particularly, the combination of DZ1+2 appeared to be the most efficient for *CDR1as* regulation (Fig. 5e), consistent with the result of transfected DZ (Fig. 3b). The combination of DZ1+2 was utilized for the synthesis of DZ@ZIF-8 complex in the subsequent experiment. The result indicated that DZ@ZIF-8 could downregulate *CDR1as* without the need of supplement of Zn^{2+}. Then, the mRNA levels of downstream genes *RAF1* and *PIK3CD* were examined. DZ@ZIF-8 could downregulate the expression levels of both downstream genes to approximately 40% (Fig. 5f). To demonstrate the versatility of this DZ-based strategy for circRNA regulation, the nanocomplex containing 10-23 DZ (10DZ) targeting

Site 1 and Site 2 on *CDR1as* was synthesized. Similarly, in the presence of Mg^{2+}, the 10DZ1+2@ZIF-8 complex could also downregulate the RNA levels of *CDR1as* and the mRNA levels of downstream *RAF1* and *PIK3CD* (Figs. S5e and S5f).

2.4 Construction and application of dual-functional DZ/MB@ZIF-8 in live cells

DZ@ZIF-8 could downregulate the RNA levels of *CDR1as*, liberating sequestered miR-7. This derepression of miR-7 led to the inhibition of its downstream oncogenic targets (e.g., *RAF1* and *PIK3CD*). Therefore, by introducing a miR-7-targeting MB, we could achieve simultaneous optical observation of the nanoplatform's activity (Fig. 6a). With the predictive assistance of MXfold2 (http://ws.sato-lab.org/mxfold2) and RNAstructure software, a molecule beacon complementary to miR-7 was designed, with a fluorescent group Cy3 and a quenching group black hole quencher-2 (BHQ-2) modified at its two ends, respectively (Fig. S6a). Recognition and binding between miR-7 and the miR-7-targeting MB was confirmed by gel electrophoresis (Fig. S6b). Next, the MB probe was incubated with miR-7 at gradually increasing concentrations from 0 to 200 nmol/L, and the fluorescence was measured. The results showed that the fluorescence intensity increased accordingly with the concentration of miR-7 (Fig. 6b).

Having validated the efficiency of MB in miR-7 detection, we constructed a dual-functional ZIF-8-based nanocomplex co-encapsulating DZ and MB, in which DZ can cleave *CDR1as*, and MB is responsible for evaluating the cleavage outcome by monitoring miR-7 levels. DZ/MB@ZIF-8 was synthesized and incubated with MCF-7 cells. The expression levels of the *CDR1as*/miR-7 axis were measured by RT-qPCR. Indeed, DZ/MB@ZIF-8 treatment downregulated *CDR1as* levels and caused an increase in miR-7 accordingly (Figs. 6c, 6d, and S6c). Notably, DZ/MB@ZIF-8 was more efficient in upregulating miR-7 than an equal amount of DZ that was transfected via a transfection reagent and supplemented with Zn^{2+}, demonstrating the superiority of ZIF-8 to provide both effective DZ delivery and supply of essential Zn^{2+} cofactor.

To ensure that the fluorescence readout provides a quantitatively robust reflection of miR-7 levels without saturating the sensor, the nanoplatform was engineered to load MBs in a significant excess relative to the expected physiological miR-7 fluctuations. The reliability of this optical signal was further validated. Control experiments confirmed that the presence of MB did not interfer with the reverse transcription or amplification efficiency of miR-7, and the robust fluorescence turn-on observed in live cells closely mirrored the miR-7 upregulation detected via RT-qPCR (Fig. S6c). Furthermore, the fluorescence properties of the Cy3 fluorophore remained highly stable across a pH range from 5.0 to 8.0 (Fig. S5d), eliminating the possibility of pH-induced artifacts during lysosomal degradation. Notably, while free DZ delivered by Lipofectamine 3000 (DZ/MB@Lipo3000) could also cleave *CDR1as*, its efficiency was slightly lower than that achieved by DZ/MB@ZIF-8 (Fig. 6c).

Next, we explored DZ/MB@ZIF-8 for its capacity to monitor miR-7 in live cells. Upon treatment with DZ/MB@ZIF-8, obvious fluorescence signals could be observed. In contrast, cells treated with MB@ZIF-8 nanocomplex showed no fluorescence, demonstrating that DZ cleavage is necessary for miR-7 release (Fig. 6e). Concurrently, the results of flow cytometry analysis demonstrated a significant enhancement of intracellular fluorescence only in cells incubated with complex DZ/MB@ZIF-8 (Fig. 6f). When a bifunctional nanocomplex based on 10-23 DZ (10DZ/MB@ZIF-8) was applied to MCF-7 cells in the presence of Mg^{2+}, both the downregulation of *CDR1as* RNA levels and increased fluorescence of miR-7 were observed (Fig. S6d and S6e).

Finally, the applicability of DZ/MB@ZIF-8 was investigated in cell lines other than MCF-7 cells. Human glioblastoma multiforme cells (U87MG) and human embryonic kidney cells (HEK293T) were treated with DZ/MB@ZIF-8 and analyzed for *CDR1as* abundance and miR-7 imaging. DZ/MB@ZIF-8 could efficiently downregulate the RNA levels of *CDR1as* in both cells and showed increased fluorescence, as determined by flow cytometry analysis and confocal microscopy (Fig. 7). The bifunctional nanocomplex 10DZ/MB@ZIF-8 was also applied to U87MG and HEK293T cells in the presence of Mg^{2+}. The downregulation of *CDR1as* RNA levels and increased fluorescence of miR-7 were also observed (Fig. S7). Therefore, the DZ-based strategy for simultaneous *CDR1as* cleavage and miR-7 imaging exhibited excellent universality, adapting well to nanocomplexes constructed from various DZs and proving applicable to multiple cell lines.

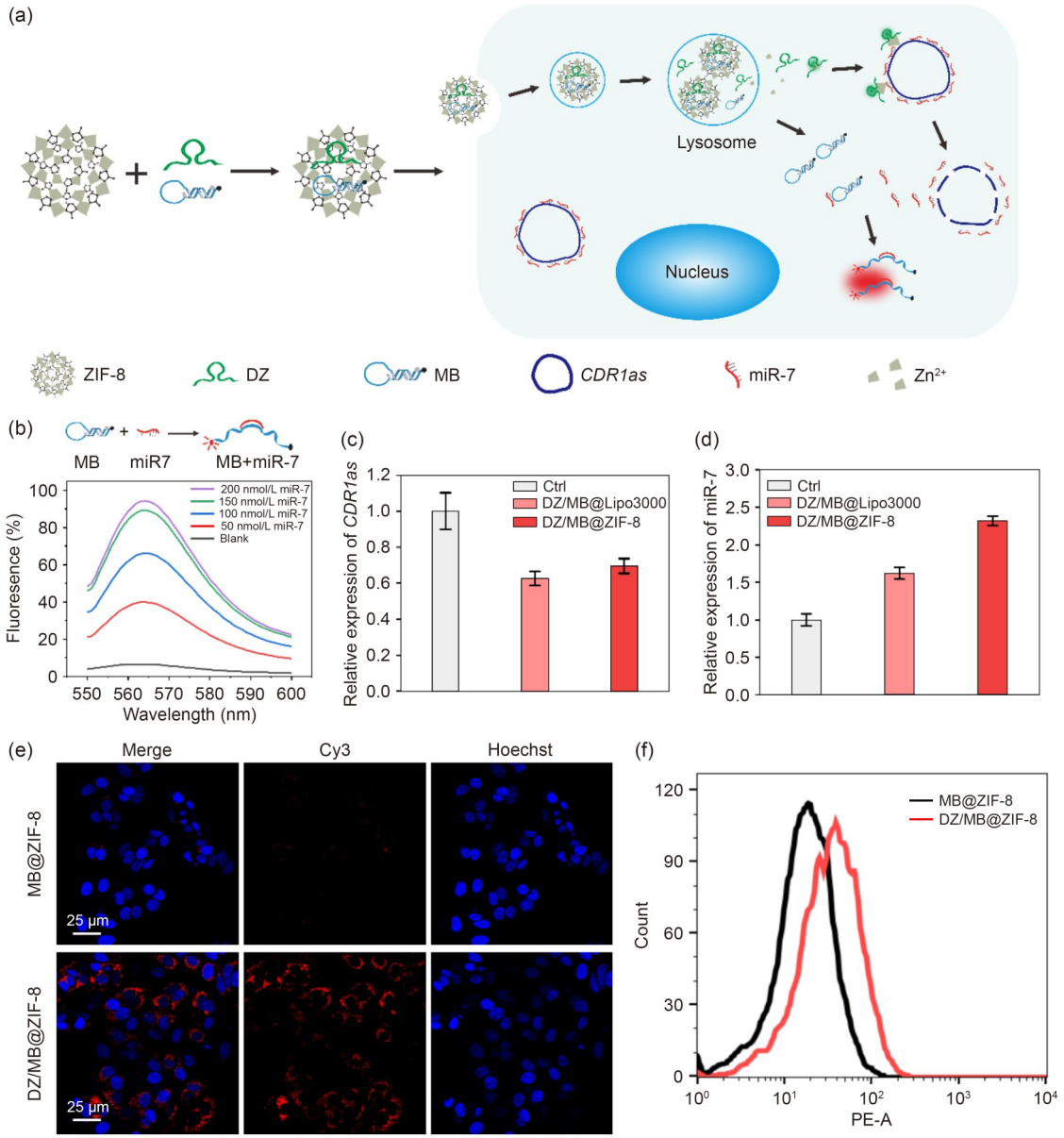


Fig. 6 Regulation and monitoring of the *CDR1as*/miR-7 axis by DZ/MB@ZIF-8. (a) Schematic diagram of the intracellular process of DZ/MB@ZIF-8-mediated *CDR1as* cleavage and miR-7 sensing. (b) Fluorescence spectra of MB incubated with different concentrations of miR-7. (c) Levels of *CDR1as* treated with DZ/MB@ZIF-8 determined by RT-qPCR. (d) Levels of miR-7 treated with DZ/MB@ZIF-8 determined by RT-qPCR. (e) Confocal images of MCF-7 cells treated with MB@ZIF-8 or DZ/MB@ZIF-8 (Cy3: red; Hoechst: blue). (f) Intracellular fluorescence intensity of MCF-7 cells treated with MB@ZIF-8 or DZ/MB@ZIF-8 measured by flow cytometry. (c, d) The data are presented as mean±SD from three independent biological replicates. ZIF-8: zeolitic imidazolate framework-8; DZ: DNAzyme; Cy3: cyanine 3; MB: molecular beacon; miR-7: microRNA-7; *CDR1as*: cerebellar degeneration-related protein 1 antisense; Lipo3000: Lipofectamine 3000; RT-qPCR: reverse transcription quantitative polymerase chain reaction; PE-A: phycoerythrin-area.

3 Conclusions

In summary, we have developed a versatile theranostic nanoplatform, DZ/MB@ZIF-8, for the simultaneous regulation and real-time monitoring of the oncogenic circRNA *CDR1as* and its downstream pathway. This system elegantly co-delivers a synergistic DZ set for the efficient cleavage of *CDR1as* and an MB for miR-7 detection. The ZIF-8 carrier is not merely a passive vehicle; its pH-responsive degradation in

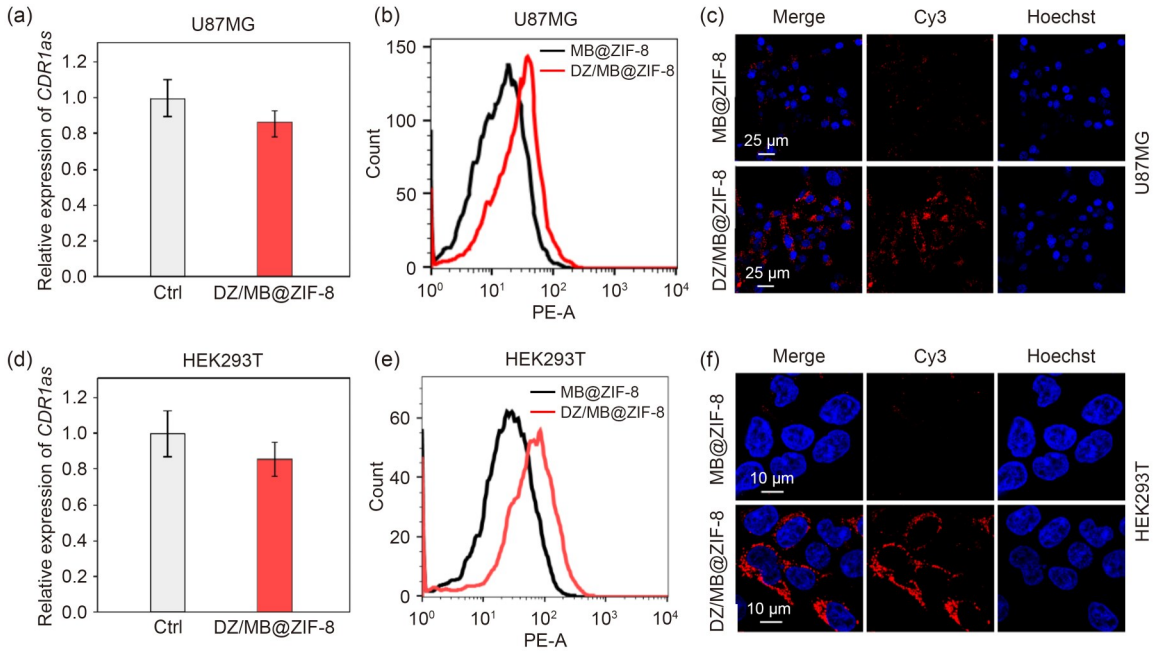


Fig. 7 Regulation and monitoring of the *CDR1as*/miR-7 axis in multiple cell lines by DZ/MB@ZIF-8. (a, d) RNA levels of *CDR1as* in U87MG (a) and HEK293T (d) cells treated with DZ/MB@ZIF-8 determined by RT-qPCR. The data are presented as mean±SD from three independent biological replicates. (b, e) Intracellular fluorescence intensity of U87MG (b) and HEK293T (e) cells treated with MB@ZIF-8 or DZ/MB@ZIF-8 measured by flow cytometry. (c, f) Confocal images of U87MG (c) and HEK293T (f) cells treated with MB@ZIF-8 or DZ/MB@ZIF-8 (Cy3: red; Hoechst: blue). Ctrl: control; ZIF-8: zeolitic imidazolate framework-8; Cy3: cyanine 3; DZ: DNAzyme; MB: molecular beacon; miR-7: microRNA-7; *CDR1as*: cerebellar degeneration-related protein 1 antisense; RT-qPCR: reverse transcription quantitative polymerase chain reaction; PE-A: phycoerythrin-area.

lysosomes ensures triggered release of the functional agents while also supplying essential Zn^{2+} cofactors for optimal DZ activity.

We have demonstrated that the targeted degradation of *CDR1as* derepresses miR-7, leading to the subsequent downregulation of key oncogenic targets, *RAF1* and *PIK3CD*. Crucially, this therapeutic effect is coupled with a direct, real-time fluorescent readout via the miR-7-sensing MB, enabling live-cell visualization of the platform's efficacy. The broad applicability of this approach was further validated across multiple cell lines and with alternative DZ designs.

Overall, this work establishes a powerful strategy for the real-time functional analysis of circRNAs, moving beyond simple knockdown to integrated perturbation and validation. By providing a direct window into the dynamic circRNA-miRNA-mRNA regulatory network, our DZ/MB@ZIF-8 nanoplatform presents a promising tool for fundamental biological discovery and advances the development of circRNA-targeted cancer therapeutics.

Materials and methods

Detailed methods are provided in the electronic supplementary materials of this paper.

Data availability statement

The data that support the findings of this study are available from the corresponding authors upon reasonable request.

Acknowledgments

This work was supported by the Natural Science Foundation of Shanghai (No. 24ZR1455600) and the National Natural Science Foundation of China (No. 21974089).

Author contributions

Nan CHEN conceived the study, coordinated the scientific team, and wrote and edited the manuscript; Yan HUANG, Jialin YE, and Lan XU performed the experimental research and data analysis, and wrote and edited the manuscript. Xingjie HU contributed to the study design, data analysis, and writing and editing of the manuscript. All authors have read and approved the final manuscript, and therefore, have full access to all the data in the study and take responsibility for the integrity and security of the data.

Compliance with ethics guidelines

Yan HUANG, Jialin YE, Lan XU, Xingjie HU, and Nan CHEN declare that they have no conflicts of interest.

This article does not contain any studies with human or animal subjects performed by any of the authors.

Declaration on the use of generative AI tools

No generative AI tools were used in the preparation of this manuscript.

References

Agarwal V, Bell GW, Nam JW, et al., 2015. Predicting effective microRNA target sites in mammalian mRNAs. *eLife*, 4:e05005. https://doi.org/10.7554/eLife.05005

Ashwal-Fluss R, Meyer M, Pamudurti NR, et al., 2014. CircRNA biogenesis competes with pre-mRNA splicing. *Mol Cell*, 56(1):55-66. https://doi.org/10.1016/j.molcel.2014.08.019

Behr M, Zhou J, Xu B, et al., 2021. *In vivo* delivery of CRISPR-Cas9 therapeutics: progress and challenges. *Acta Pharm Sin B*, 11(8):2150-2171. https://doi.org/10.1016/j.apsb.2021.05.020

Bloomer H, Khirallah J, Li YM, et al., 2022. CRISPR/Cas9 ribonucleoprotein-mediated genome and epigenome editing in mammalian cells. *Adv Drug Deliv Rev*, 181:114087. https://doi.org/10.1016/j.addr.2021.114087

Breuer J, Barth P, Noe Y, et al., 2022. What goes around comes around: artificial circular RNAs bypass cellular antiviral responses. *Mol Ther Nucleic Acids*, 28:623-635. https://doi.org/10.1016/j.omtn.2022.04.017

Cepeda-Plaza M, Peracchi A, 2020. Insights into DNA catalysis from structural and functional studies of the 8-17 DNAzyme. *Org Biomol Chem*, 18(9):1697-1709. https://doi.org/10.1039/c9ob02453k

Chen H, Mao M, Jiang J, et al., 2019. Circular RNA CDR1as acts as a sponge of miR-135b-5p to suppress ovarian cancer progression. *Onco Targets Ther*, 12:3869-3879. https://doi.org/10.2147/ott.S207938

Chen KD, Xu YT, Li JX, et al., 2025. The potential and challenges of circular RNA in the development of vaccines and drugs for emerging infectious diseases. *Mol Ther Nucleic Acids*, 36(3):102687. https://doi.org/10.1016/j.omtn.2025.102687

Fan SH, Ma C, Tian XP, et al., 2021. Detection of *Vibrio vulnificus* in seafood with a DNAzyme-based biosensor. *Front Microbiol*, 12:655845. https://doi.org/10.3389/fmicb.2021.655845

Feng C, Che XR, Mao CQ, et al., 2025. Enhanced DNAzyme-based tetrahedron amplifier for ultrasensitive determination and intracellular imaging of breast cancer-related microRNAs. *ACS Sens*, 10(11):8895-8905. https://doi.org/10.1021/acssensors.5c02856

Gao WY, Han XP, Li L, et al., 2025. Functionalized ZIF-8 as a versatile platform for drug delivery and cancer therapy: strategies, challenges and prospects. *J Mater Chem B*, 13(12):3758-3785. https://doi.org/10.1039/d4tb02289k

Hansen TB, Jensen TI, Clausen BH, et al., 2013. Natural RNA circles function as efficient microRNA sponges. *Nature*, 495(7441):384-388. https://doi.org/10.1038/nature11993

Jeck WR, Sorrentino JA, Wang K, et al., 2013. Circular RNAs are abundant, conserved, and associated with ALU repeats. *RNA*, 19(2):141-157. https://doi.org/10.1261/rna.035667.112

Lee M, Kang S, Kim S, et al., 2023. Advances and trends in miRNA analysis using DNAzyme-based biosensors. *Biosensors*, 13(9):856. https://doi.org/10.3390/bios13090856

Li CC, Xu TY, Hou GP, et al., 2025. DNA nanotechnology-based strategies for gastric cancer diagnosis and therapy. *Mater Today Bio*, 30:101459. https://doi.org/10.1016/j.mtbio.2025.101459

Li R, Xu XJ, Gao S, et al., 2023. Circular RNA CDR1as mediated by human antigen R (HuR) promotes gastric cancer growth via miR-299-3p/TGIF1 axis. *Cancers*, 15(23):5556. https://doi.org/10.3390/cancers15235556

Liu CX, Chen LL, 2022. Circular RNAs: characterization, cellular roles, and applications. *Cell*, 185(12):2016-2034. https://doi.org/10.1016/j.cell.2022.04.021

Liu QL, Zhang Z, Wei XW, et al., 2021. Noncoding RNAs in tumor metastasis: molecular and clinical perspectives. *Cell Mol Life Sci*, 78(21-22):6823-6850. https://doi.org/10.1007/s00018-021-03929-0

Liu QW, He Y, Xu WW, 2022. Molecular functions and therapeutic applications of exosomal noncoding RNAs in cancer. *Exp Mol Med*, 54(3):216-225. https://doi.org/10.1038/s12276-022-00744-w

Liu RD, Li JX, Salena BJ, et al., 2025. Aptamer and DNAzyme based colorimetric biosensors for pathogen detection. *Angew Chem Int Ed*, 64(4):e202418725. https://doi.org/10.1002/anie.202418725

Mao XJ, Cao YY, Guo ZJ, et al., 2021. Biological roles and therapeutic potential of circular RNAs in osteoarthritis. *Mol Ther Nucleic Acids*, 24:856-867. https://doi.org/10.1016/j.omtn.2021.04.006

McConnell EM, Cozma I, Mou QB, et al., 2021. Biosensing with DNAzymes. *Chem Soc Rev*, 50(16):8954-8994. https://doi.org/10.1039/d1cs00240f

Mehta SL, Chokkalla AK, Bathula S, et al., 2023. CDR1as regulates α-synuclein-mediated ischemic brain damage by controlling miR-7 availability. *Mol Ther Nucleic Acids*, 31:57-67. https://doi.org/10.1016/j.omtn.2022.11.022

Meng LJ, Ding PA, Liu SH, et al., 2020. The emerging prospects of circular RNA in tumor immunity. *Ann Transl Med*, 8(17):1091. https://doi.org/10.21037/atm-19-4751

Mishra NO, Quon AS, Nguyen A, et al., 2023. Constructing physiological defense systems against infectious disease with metal–organic frameworks: a review. *ACS Appl Bio Mater*, 6(8):3052-3065.

https://doi.org/10.1021/acsabm.3c00391

Nurmi C, Gu J, Mathai A, et al., 2024. Making target sites in large structured RNAs accessible to RNA-cleaving DNAzymes through hybridization with synthetic DNA oligonucleotides. *Nucleic Acids Res*, 52(18):11177-11187. https://doi.org/10.1093/nar/gkae778

Odame E, Li L, Nabilla JA, et al., 2023. miR-145-3p inhibits MuSCs proliferation and mitochondria mass via targeting MYBL1 in Jianzhou big-eared goats. *Int J Mol Sci*, 24(9):8341. https://doi.org/10.3390/ijms24098341

Piwecka M, Glažar P, Hernandez-Miranda LR, et al., 2017. Loss of a mammalian circular RNA locus causes miRNA deregulation and affects brain function. *Science*, 357(6357): eaam8526. https://doi.org/10.1126/science.aam8526

Ruda VM, Chandwani R, Sehgal A, et al., 2014. The roles of individual mammalian argonautes in RNA interference *in vivo*. *PLoS One*, 9(7):e101749. https://doi.org/10.1371/journal.pone.0101749

Santoro SW, Joyce GF, 1997. A general purpose RNA-cleaving DNA enzyme. *Proc Natl Acad Sci USA*, 94(9):4262-4266. https://doi.org/10.1073/pnas.94.9.4262

Sato K, Akiyama M, Sakakibara Y, 2021. RNA secondary structure prediction using deep learning with thermodynamic integration. *Nat Commun*, 12:941. https://doi.org/10.1038/s41467-021-21194-4

Schubert S, 2003. RNA cleaving '10-23' DNAzymes with enhanced stability and activity. *Nucleic Acids Res*, 31(20): 5982-5992. https://doi.org/10.1093/nar/gkg791

Shafaghat Z, Radmehr S, Saharkhiz S, et al., 2025. Circular RNA, a molecule with potential chemistry and applications in RNA-based cancer therapeutics: an insight into recent advances. *Top Curr Chem*, 383(2):21. https://doi.org/10.1007/s41061-025-00505-z

Shao YC, Xu JZ, Liang B, et al., 2023. The role of CDR1as/ciRS-7 in cardio-cerebrovascular diseases. *Biomed Pharm*, 167:115589. https://doi.org/10.1016/j.biopha.2023.115589

Singh RR, Mondal I, Janjua T, et al., 2024. Engineered smart materials for RNA based molecular therapy to treat Glioblastoma. *Bioact Mater*, 33:396-423. https://doi.org/10.1016/j.bioactmat.2023.11.007

Song GX, Tian CH, Li JH, et al., 2023. Rapid characterization of anti-CRISPR proteins and optogenetically engineered variants using a versatile plasmid interference system. *Nucleic Acids Res*, 51(22):12381-12396. https://doi.org/10.1093/nar/gkad995

Troyano J, Carné-Sánchez A, Avci C, et al., 2019. Colloidal metal–organic framework particles: the pioneering case of ZIF-8. *Chem Soc Rev*, 48(23):5534-5546. https://doi.org/10.1039/c9cs00472f

Victor J, Steger G, Riesner D, 2018. Inability of DNAzymes to cleave RNA in vivo is due to limited Mg^{2+} concentration in cells. *Eur Biophys J*, 47(4):333-343. https://doi.org/10.1007/s00249-017-1270-2

Wang HM, Chen YQ, Wang H, et al., 2019. DNAzyme-loaded metal–organic frameworks (MOFs) for self-sufficient gene therapy. *Angew Chem Int Ed*, 58(22):7380-7384. https://doi.org/10.1002/anie.201902714

Wang W, Sun L, Huang MT, et al., 2023. Regulatory circular RNAs in viral diseases: applications in diagnosis and therapy. *RNA Biol*, 20(1):847-858. https://doi.org/10.1080/15476286.2023.2272118

Wei KJ, He MY, Zhang J, et al., 2023. A DNA logic circuit equipped with a biological amplifier loaded into biomimetic ZIF-8 nanoparticles enables accurate identification of specific cancers in vivo. *Angew Chem Int Ed*, 62(41): e202307025. https://doi.org/10.1002/anie.202307025

Wightman FF, Lukin J, Giusti SA, et al., 2024. Influence of RNA circularity on target RNA-directed microRNA degradation. *Nucleic Acids Res*, 52(6):3358-3374. https://doi.org/10.1093/nar/gkae094

Wu D, Liu X, Tang LJ, et al., 2024. Three-way junction-mediated three-letter coded SDA cascade CRISPR/Cas12a system for circRNA detection. *Chem Eng J*, 497:154542. https://doi.org/10.1016/j.cej.2024.154542

Wu SX, Zhang KX, Liang Y, et al., 2022. Nano-enabled tumor systematic energy exhaustion via zinc (II) interference mediated glycolysis inhibition and specific GLUT1 depletion. *Adv Sci*, 9(7):2103534. https://doi.org/10.1002/advs.202103534

Xu B, Yang TY, Wang Z, et al., 2018. CircRNA CDR1as/miR-7 signals promote tumor growth of osteosarcoma with a potential therapeutic and diagnostic value. *Cancer Manag Res*, 10:4871-4880. https://doi.org/10.2147/cmar.S178213

Xu C, Xu YH, Wang GM, 2025. Bibliometric analysis of research on cervical cancer and miRNAs from 2010 to 2024: research trends, hotspots, and prospects. *Discov Oncol*, 16:1639. https://doi.org/10.1007/s12672-025-03106-w

Yang J, Meng XD, Pan JC, et al., 2018. CRISPR/Cas9-mediated noncoding RNA editing in human cancers. *RNA Biol*, 15(1): 35-43. https://doi.org/10.1080/15476286.2017.1391443

Yang XQ, Ye T, Liu HR, et al., 2021. Expression profiles, biological functions and clinical significance of circRNAs in bladder cancer. *Mol Cancer*, 20:4. https://doi.org/10.1186/s12943-020-01300-8

Ye JC, Xie C, Wang CL, et al., 2021. Promoting musculoskeletal system soft tissue regeneration by biomaterial-mediated modulation of macrophage polarization. *Bioact Mater*, 6(11):4096-4109. https://doi.org/10.1016/j.bioactmat.2021.04.017

Yu H, Zhao Q, 2023. DNAzyme-based microscale thermophoresis sensor. *Anal Chem*, 95(4):2152-2156. https://doi.org/10.1021/acs.analchem.2c04643

Zeng ZH, Zhong MZ, Liao T, et al., 2024. Nano-fuels-driven self-sacrificed ZIF-8@Apt integrated chip coupled with a DNAzyme system for the isolation and detection of glioblastoma-derived extracellular vesicles. *Chem Eng J*, 502:157445. https://doi.org/10.1016/j.cej.2024.157445

Zhang XY, Liu QB, Zhang TT, et al., 2022. Bone-targeted nanoplatform enables efficient modulation of bone tumor microenvironment for prostate cancer bone metastasis treatment. *Drug Deliv*, 29(1):889-905. https://doi.org/10.1080/10717544.2022.2050845

Zhang YJ, Huang XW, Wang LS, et al., 2021. Glutathionylation-dependent proteasomal degradation of wide-spectrum mutant p53 proteins by engineered zeolitic imidazolate framework-8. *Biomaterials*, 271:120720. https://doi.org/10.1016/j.biomaterials.2021.120720

Zhang YT, Hu JP, Qu XY, et al., 2023. Circular RNA RSU1 promotes retinal vascular dysfunction by regulating miR-345-3p/TAZ. *Commun Biol*, 6:719. https://doi.org/10.1038/s42003-023-05064-x

Zhao X, Cheng H, Wang QW, et al., 2023. Regulating photosensitizer metabolism with DNAzyme-loaded nanoparticles for amplified mitochondria-targeting photodynamic immunotherapy. *ACS Nano*, 17(14):13746-13759. https://doi.org/10.1021/acsnano.3c03308

Zuker M, 2003. Mfold web server for nucleic acid folding and hybridization prediction. *Nucleic Acids Res*, 31(13): 3406-3415. https://doi.org/10.1093/nar/gkg595

Supplementary information

Materials and methods; Figs. S1–S7; Tables S1 and S2